

Simulations of Shor's algorithm with implications to scaling and quantum error correction.

Simon J. Devitt, Austin G. Fowler and Lloyd C. L. Hollenberg.

Centre for Quantum Computer Technology, School of Physics

University of Melbourne, Victoria 3010, Australia.

(Dated: April 8, 2019)

The publication in 1994 of Shor's algorithm, which allows factorisation of composite number N in a time polynomial in its binary length L has been the primary catalyst for the race to construct a functional quantum computer. However, it seems clear that any practical system that may be developed will not be able to perform completely error free quantum gate operations or shield even idle qubits from inevitable error effects. Hence, the practicality of quantum algorithms needs to be investigated to not only determine limitations on such algorithms in a noisy quantum computer, but also to estimate what demands must be made of quantum error correction (QEC). Shor's algorithm is a combination of both classical pre and post-processing, and also a quantum period finding subroutine (QPF) which allows for the exponential speed up of this algorithm on a quantum device. This paper will look at the stability of this quantum subroutine under the effects of several error models. Direct simulation of the entire QPF subroutine required to factorise a given composite number N in the presence of errors shows that the circuit required to implement Shor's algorithm is very sensitive to a small number of errors within the entire calculation. Well designed and efficient error correction codes, quick gate times and very low gate error rates will be essential for any physical realisation of Shor's factoring algorithm.

Since Shor's discovery of a factoring algorithm, which on a quantum computer can factor large numbers in polynomial time [1], a large international effort is attempting to construct a practical quantum computer. Currently there are many different proposals for constructing such a device [2, 3]. However despite all these efforts it has so far proved to be a difficult process to control qubits and to shield them from various types of quantum decoherence. For this reason it is imperative to investigate the practicality of large scale quantum circuits in order to answer the fundamental question of whether these algorithms be implemented on a physically realistic quantum computer?

Quantum error correction (QEC), fault tolerant quantum computation (FTQC) and concatenated codes [2, 4, 5] can offer a method to reduce the damage on quantum circuits caused by error effects. However, implementation of such schemes often require large numbers of qubits (which can grow quite quickly if a particular quantum circuit requires several levels of concatenated error correction) and complicated quantum circuits to produce simple fault tolerant gates [2]. Hence, a detailed analysis of error stability for Shor's algorithm is a must to provide a reasonable estimate of QEC requirements for any realistic implementation of the algorithm. Several authors have previously examined the effects of errors on Shor's algorithm [6, 7, 13]. However, these simulations often limit the investigation to specific sections of the entire circuit, or to other sources of error such as phase drifts on idle qubits, imperfect gate operations or aspects relating to quantum chaos. This paper will look at an entire circuit for full implementation of the quantum period finding subroutine and two specific types of error models discussed below.

Shor's algorithm provides an ingenious method for factoring large numbers, however, it assumes that the user has access to a quantum computer free from all error effects. This is an unrealistic requirement. It has become clear that any

physical quantum computer will not be completely isolated from the environment, and that implementation of certain quantum gates cannot be implemented with 100% accuracy. In order to assess the viability of Shor's algorithm we need to answer the following:

1. How does the probability of success for the QPF subroutine depend on various errors?
2. Does the restriction of nearest neighbour qubit interactions have a major effect on the stability of the quantum circuit?
3. What implications does the stability of the quantum circuit have in relation to quantum error correction?

This paper will focus on the quantum period finding subroutine (QPF), which lies at the heart of Shor's factoring algorithm and is discussed shortly. We will look at how the probability of success for this subroutine varies as we alter the size of the period finding problem. In this way we can estimate the demands on QEC for large factorisation problems, and hopefully determine if the implementation of large scale quantum circuits such as Shor's algorithm on currently proposed architectures is possible.

Section I will briefly examine the underlying theory behind Shor's algorithm, the QPF subroutine and how we will define success. Section II will involve looking at the two primary error models that we will use in this investigation and issues relating to simulations. Sections III, IV and V present our results. Several different simulations will show exactly how the QPF subroutine behaves under these two specific error models. We will examine how the subroutine scales with problem size while maintaining a fixed success rate and also how this success rate scales when we expose the circuit to a specific number of error gates. Section VI will relate results back to the demands on QEC and concatenated codes.

I. SHOR'S ALGORITHM

As several papers detail the major steps of Shor's algorithm [1, 8, 9], we will only give a brief overview for the sake of completeness. We first consider a given composite number $N = N_1 N_2$ which has a binary length $L = \log_2(N)$. In order to factorise this number we consider the function $f(k) = x^k \bmod N$, where $k = 1, 2, 3, \dots$ and x is a randomly chosen integer such that $1 < x < N$ and $\gcd(N, x) = 1$ ($\gcd \equiv$ greatest common divisor). The QPF subroutine of Shor's algorithm is designed to determine the period of $f(k)$. i.e, to find the integer $r > 0$ such that $f(r) = 1$. This QPF subroutine is the quantum component of Shor's algorithm. The complete algorithm is composed of both the QPF subroutine and several pre and post processing operations that can be performed in polynomial time using classical techniques. These classical steps are detailed by several authors [1, 2, 9], however they are not important for this investigation and hence will not be discussed. Once the QPF subroutine returns a value for the period of $f(k)$ the factors of N can be calculated as $N_1 = \gcd(f(r/2) - 1, N)$ and $N_2 = \gcd(f(r/2) + 1, N)$. This is conditional on r being even and $f(r/2) \neq N - 1$. It can be shown [2] that a randomly chosen x will result in the QPF algorithm returning non-trivial factors of N , with probability $1 - 1/2^t$. Where t is the number of distinct prime factors of N . Given N is a product of two primes, we find that in the absence of errors the QPF subroutine still determines a useful value of r , for a random choice of x , with probability = 0.75.

Many circuits have been proposed in order to implement the QPF subroutine on a physical quantum computer, as summarised in table I. Some are optimised for conceptual

Circuit	Qubits	Depth
Simplicity [10]	$\sim 5L$	$O(L^3)$
Speed [11]	$O(L^2)$	$O(L \log L)$
Qubits [12]	$\sim 2L$	$\sim 32L^3$
Tradeoff 1 [14]	$\sim 50L$	$\sim 2^{19} L^{1.2}$
Tradeoff 2 [14]	$\sim 5L$	$\sim 3000L^2$

TABLE I: Number of qubits required and circuit depth of different implementations of the QPF subroutine. Where possible, figures are accurate to leading order in L .

simplicity, some for speed and some for utilising a minimum number of qubits. This investigation will focus on circuits that require a minimal number of qubits for two reasons. Firstly, scalability of quantum computer architectures implies that circuits requiring as few qubits as possible are desirable. Secondly, classical simulations of quantum circuits become difficult when manipulating large numbers of qubits. Beauregard [12] details an implementation of the QPF subroutine for a quantum computer that can interact any two qubits simultaneously. However, a large number of architectures are restricted to a single line of qubits that can interact nearest neighbours only. Generally these architectures allow multiple pairs of qubits to be interacted at the same time, provided all these pairs are isolated. We will refer to these as Linear

Nearest Neighbour (LNN) architectures. A comprehensive paper detailing the LNN circuit used in this investigation can be found in [15] with figures (7, 8,9 and 10) showing certain sections of the circuit discussed later. While it may appear that any LNN circuit would require many more gate operations to implement the QPF subroutine than an equivalent circuit employing arbitrary interactions, if we add one extra qubit to the Beauregard circuit eliminating the need for doubly controlled Fourier addition gates, both the LNN circuit and the Beauregard circuit require $2L + 4$ qubits and have identical depths and gate counts to leading order in L .

Next, we detail how we define success of the QPF subroutine. The underlying steps to factorise a number of binary length L first requires the initialisation of $3L$ qubits to the state $|0\rangle_{2L}|0\rangle_L$. The actual number of qubits used in our circuit is less than this since we replace the $2L$ qubit register with a single master control qubit that is sequentially measured $2L$ times. This replacement does not effect the following analysis which is performed on the full $3L$ qubit computer. For clarity we have broken these $3L$ qubits into a $2L$ qubit k register and a L qubit f register. The next step requires a Hadamard transform to be performed on each qubit in the k register,

$$|0\rangle_{2L}|0\rangle_L \longrightarrow \frac{1}{2^L} \sum_{k=0}^{2^{2L}-1} |k\rangle_{2L}|0\rangle_L. \quad (1)$$

Step three is to apply the function $f(k)$ on the f register, conditional on the values of the k register. The resultant state of the computer is,

$$\frac{1}{2^L} \sum_{k=0}^{2^{2L}-1} |k\rangle_{2L}|0\rangle_L \longrightarrow \frac{1}{2^L} \sum_{k=0}^{2^{2L}-1} |k\rangle_{2L}|x^k \bmod N\rangle_L. \quad (2)$$

Next we measure the f register. This step can actually be omitted. We present it here to show explicitly how the period r appears within this procedure. After measurement we obtain,

$$\frac{1}{2^L} \sum_{k=0}^{2^{2L}-1} |k\rangle_{2L}|f(k)\rangle_L \longrightarrow \frac{\sqrt{r}}{2^L} \sum_{n=0}^{2^{2L}/r-1} |k_0 + nr\rangle_{2L}|f_0\rangle_L. \quad (3)$$

Where r is the period of f , f_0 is the measured value and k_0 is the smallest value of k such that $f_0 = f(k_0)$. We now apply a quantum Fourier transform (QFT) to the k register. The state of the computer after the application of the QFT becomes,

$$\frac{\sqrt{r}}{2^{2L}} \sum_{j=0}^{2^{2L}-1} \sum_{n=0}^{2^{2L}/r-1} \exp\left(\frac{2i\pi}{2^{2L}} j(k_0 + nr)\right) |j\rangle_{2L}|f_0\rangle_L. \quad (4)$$

If we now measure the k register, we will return a value of j with probability given by,

$$Pr(j, r, L) = \left| \frac{\sqrt{r}}{2^{2L}} \sum_{n=0}^{2^{2L}/r-1} \exp\left(\frac{2i\pi}{2^{2L}} jnr\right) \right|^2. \quad (5)$$

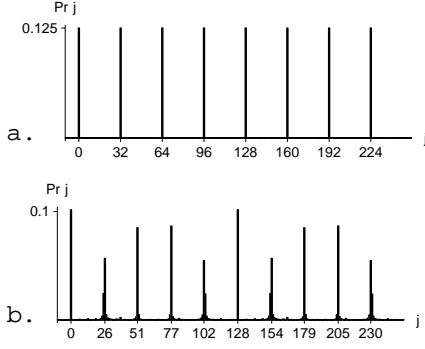


FIG. 1: Plot of equation 5 for the case, $2^{2L} = 256$ with a) $r = 8$ and b) $r = 10$.

Equation (5) is strongly peaked at certain values of j . If the period r perfectly divides 2^{2L} then (5) can be evaluated exactly, with the probability of observing $j = c2^{2L}/r$ for $0 \leq c < r$ being $1/r$, and 0 if $j \neq c2^{2L}/r$ [figure 1(a)]. If r is not a perfect divisor of 2^{2L} , then the peaks of equation (5) become slightly broader, [figure 1(b)]. In this case, classical methods can be utilised in order to determine r from the values measured. Various authors [2, 9] show how a continued fraction method can be used to determine r , given several measured integer values around these non-integer peaks. Hence, we define the probability of success s for Shor's algorithm as,

$$s(L, r) = \sum_{\{useful\ j\}} Pr(j, L, r), \quad (6)$$

where $\{useful\ j\}$ is the set, $j = \lfloor c2^{2L}/r \rfloor$, $j = \lceil c2^{2L}/r \rceil$, $0 < c < r$, where $\lfloor \cdot \rfloor$ $\lceil \cdot \rceil$ denote rounding down and up respectively and $Pr(j, L, r)$ is defined via equation (5). Using this definition of s we can determine the period r provided we can run the algorithm $O(1/s)$ times.

Our initial simulations fixed the value of s while adjusting the frequency of error gates occurring within the circuit. For each L , we chose x and N such that $f(k)$ had period $r = 6$ [table II]. The reason for this choice was in regards to the practicality of simulating the subroutine, as by our definition of $\{useful\ j\}$, only 10 evaluations of equation (5) are required to determine s . Larger periods would require examining more j values, and hence would require more computational time. However, we need to confirm that these 10 out of the 2^{2L} possible states encapsulates the majority of the probability distribution of equation (5). Initial simulations in the presence of no errors show that the j values examined cover approximately 74% of the total probability distribution. A further 17% occurs for the useless case of $j = 0$, with the remaining 9% representing j values not used within the definition of $\{useful\ j\}$. This approximation still remains valid as we increase L . We found that as we increase from L to $L + 1$ that the total amount of the probability distribution present in j values not in $\{useful\ j\}$ only increases by approximately $10^{-5}\%$.

We now describe the expected output of the QPF subroutine in the presence of severe errors. By referring back to the quantum circuit used for these simulations [figure 7] [15], it can be seen that j is obtained bit-by-bit via a series of sequential measurements on a master control qubit. This master qubit simulates the entire k -register. The QFT on this single qubit required by equation (4) is performed through a series of Hadamard gates and classically controlled single qubit rotations. In a more general analysis we can model the entire computer as two registers, a single master qubit and the rest of the computer. Consider the state of the computer at a point in the calculation just before the application of a controlled modular multiplication gate, where our master control qubit is in an equal superposition of $|0\rangle$ and $|1\rangle$ and the rest of the computer is some arbitrary unknown superposition,

$$|\phi\rangle = \frac{1}{\sqrt{2}}(|0\rangle_{master} + |1\rangle_{master}) \sum_{j=0}^{2^{2L}-1} \alpha_j |j\rangle_{computer}. \quad (7)$$

If we now apply the modular multiplication gate, the gate will return a new superposition state for the $|j\rangle_{computer}$ register. The co-efficients $\{\beta_j\}$ represent the new superposition obtained through the application of the modular multiplication gate with the master control qubit in the $|1\rangle$ state,

$$|\phi\rangle = \frac{1}{\sqrt{2}}|0\rangle \sum_{j=0}^{2^{2L}-1} \alpha_j |j\rangle + \frac{1}{\sqrt{2}}|1\rangle \sum_{j=0}^{2^{2L}-1} \beta_j |j\rangle. \quad (8)$$

Just before measurement of the master control we apply a classically controlled rotation (θ) on the master control qubit and a second Hadamard rotation. The value of θ is dependent on the result of all previous measurements on this qubit. Hence the state just before measurement is,

$$|\phi\rangle = \frac{1}{2}|0\rangle \sum_{j=0}^{2^{2L}-1} (\alpha_j + e^{i\theta}\beta_j)|j\rangle + \frac{1}{2}|1\rangle \sum_{j=0}^{2^{2L}-1} (\alpha_j - e^{i\theta}\beta_j)|j\rangle. \quad (9)$$

Therefore, the probability of measuring a 1 or 0 is given by,

$$P\left(\frac{1}{2} \mp \frac{1}{2}\right) = \frac{1}{2} \pm \frac{1}{4} \sum_{j=0}^{2^{2L}-1} (e^{i\theta}\alpha_j^*\beta_j + e^{-i\theta}\alpha_j\beta_j^*), \quad (10)$$

where we have used

$$\sum_{j=0}^{2^{2L}-1} |\alpha_j|^2 = \sum_{j=0}^{2^{2L}-1} |\beta_j|^2 = 1. \quad (11)$$

Errors cause the second half of equation (10) to asymptote to 0 resulting in an equal probability $P = (0.5)^{2L}$ of each j being observed. In section IV we will examine how quickly the probability of measuring a specific useful j asymptotes to this random floor as the specific number of errors in the circuit is increased.

II. ERROR MODELS AND ANALYSIS

In our simulations, we used two different error models. The first error model investigated was the set of discrete errors in which a single qubit $|\phi\rangle = \alpha|0\rangle + \beta|1\rangle$ can experience a bit flip $X|\phi\rangle$, a phase flip $Z|\phi\rangle$, or both at the same time $XZ|\phi\rangle$. Each of the three types of discrete error gates has an equal probability $p/3$ of occurring. Hence, we can examine how the success of the QPF subroutine s , depends on the probability of a discrete error occurring p , for various values of L . Within the simulations we assume perfect gate operations. All two qubit gates approximated as having the same operational times (defined as a single time step) and all single qubit gates combined with neighbouring two qubit gates via the canonical decomposition [16, 17, 18]. Discrete error gates are then applied with probability p to each qubit after each time step.

The second error model is a continuous generalisation of the discrete error case. Consider the most general $SU(2)$ matrix operating on our qubit,

$$\begin{pmatrix} \cos(\gamma/2)e^{i(\alpha+\beta)/2} & \sin(\gamma/2)e^{-i(\alpha-\beta)/2} \\ -\sin(\gamma/2)e^{i(\alpha-\beta)/2} & \cos(\gamma/2)e^{-i(\alpha+\beta)/2} \end{pmatrix}. \quad (12)$$

In order to simulate this type of error, we apply the above matrix to every qubit at each time step (including idle qubits). As with discrete errors, each gate operation is assumed to be perfect. The angles α , β and γ are distributed normally with a mean of 0 and standard deviation σ . In an analogous way to the discrete error case, we will examine how the success of the QPF subroutine s varies as we change the spread of the angle distribution, σ .

Computational times are unfortunately the major restriction on how large a circuit we can simulate. The stochastic nature of both the algorithm itself and more importantly, the application of discrete error gates required a large number of statistical runs in order to calculate a consistent average value of s for each particular value of p . Errors may or may not occur in places within the circuit that effect the final result. Hence, for a given number of statistical runs the variance on this set can be quite large. To see this in a more explicit way we can examine figure (2) which shows the effect of a single bit flip error on the value of s for the $L = 5$ circuit. Each horizontal block represents one of the 14 qubits, while each vertical slice represents a single time step where a bit flip error gate can occur. White areas indicate where the bit flip error has no effect on the success of the circuit, and successively darker regions show where bit flip errors begin to reduce the final value of s until the circuit completely fails. The image shown only represents a single modular multiplication gate and clearly shows the structure of the circuit described in [15], [figure (8,10)]. This image makes it clear that the location of the error can play a major role in the final value of s calculated, with various sections invariant to the bit flip error. The average value of s for this single section of the circuit when subjected to a single X error is $s = 0.34$.

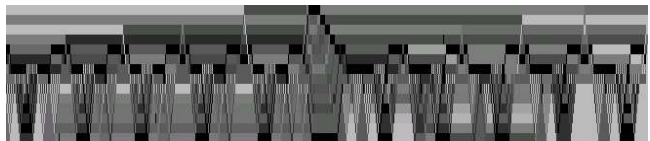


FIG. 2: Map showing how the location of a single bit flip error plays a major role in the final output success of the circuit. This image is for $L = 5$ (14 qubits), and shows the first modular multiplication section of the circuit, [figure (8)]. Darker areas represent lower values for s .

III. STABILITY WHILE MAINTAINING A FIXED RATE OF SUCCESS

The classical simulation algorithm employed to examine the QPF subroutine used a state vector representation. Matrix operations were then performed in order to simulate both quantum gates and error operations. The first section of simulations looks at how the success of the QPF subroutine s , as defined via equation (6) varies with the probability of discrete error occurring, p . Figure (3) shows the maximum value of p such that $s \approx 10\%$. The plots show the results for $2L + 4 = 14, 16, 18, 20$ and 22 , representing factorisation of composite numbers from $N = 27$ to $N = 405$. As stated earlier, for this section of simulations we examined functions that each had a period $r = 6$. Table II show the functions $f(k)$ used for each value of L . The errors in figure (3) were

$2L + 4$	$f(k) = x^k \text{mod} N$, with $r = 6$
14	$8^k \text{mod} 27$
16	$31^k \text{mod} 63$
18	$10^k \text{mod} 77$
20	$27^k \text{mod} 247$
22	$26^k \text{mod} 405$

TABLE II: Functions used for various values of L . Note that for $2L + 4 = 14, 16, 22$ the functions used are not products of two primes. With some slight modifications to the classical post-processing, Shor's algorithm can still be used to factor such numbers. Since we are only investigating the reliability of the QPF subroutine, this is not relevant to our analysis.

determined by examining a small region of p values around which $s \approx 0.1$. Raising and lowering p until the average value of s deviated by approximately 0.01 dictated our error bounds.

Analogous results for our continuous error model were determined in much the same way. In the continuous error model we again assume perfect gate operations but the 2×2 matrix shown in equation (12) is applied to every qubit at each time step. Hence, the computational time increases significantly from the discrete error case. The functions $f(k)$ used for the continuous error model are identical to the functions used for the discrete error model. Figure (4) shows our results for continuous errors, looking at the maximum value of σ such that the QPF subroutine returns a success rate of $s = 0.6$. The change to $s = 0.6$ for the continuous error model was in response to the larger simulation times required for continuous errors. The $L = 8$ circuit would require too

Shor scaling of LNN circuit subject to discrete gate errors, as L increases.

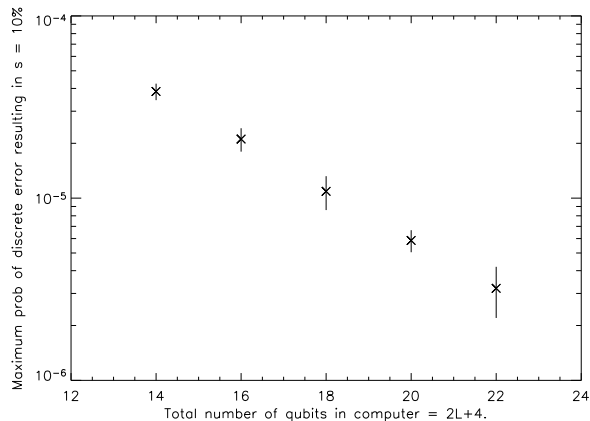


FIG. 3: Maximum probability of a discrete error occurring in our QPF circuit p , that results in a success probability of $s = 0.1$ as we increase the size of our period finding problem, L .

Shor scaling of LNN circuit subject to continuous gate errors, as L increases.

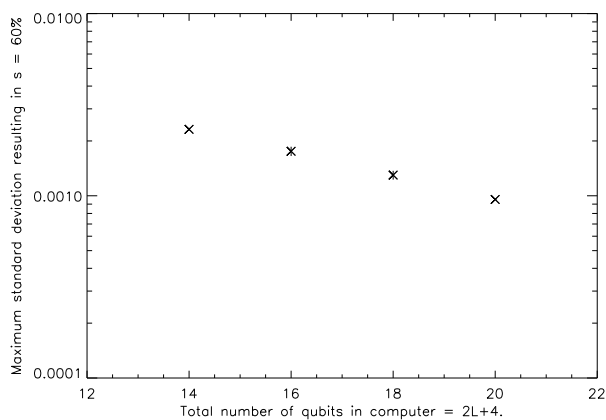


FIG. 4: Maximum spread σ of the Gaussian distribution of angles, α , β and γ that results in the QPF subroutine returning a success probability of $s = 0.6$ as we increase the size of our period finding problem, L .

much computational time in order to initially search for an approximate region for $s = 0.1$. Hence, we specified a σ value and ran the $L = 8$ simulation once returning $s = 0.6$. Appropriate σ values for $L = 5, 6, 7$ were then found since simulation times for these circuits were much shorter. For continuous errors the variance on the set of statistical runs were much smaller. Confidence limits on the data points were therefore much tighter than for the discrete error model.

Both figures show a clear exponential behaviour of the QPF subroutine. The values for p or σ returning $s = 0.1$ or $s = 0.6$ decrease quite rapidly as we increase the size of L . Naively one might expect this to be disastrous for utilising Shor's algorithm for numbers as large as those used in public key encryption. Extrapolating this behaviour out to

large L values such as $L = 128$ results in maximum error rates of the order $p = 10^{-40}$. However, referring back to the actual circuit used in the simulations [15], we see that the total area of the circuit (i.e. the number of possible locations where an error can occur) scales as $n_p = \text{number of qubits} \times \text{depth} = (2L + 4) \times (32L^3 + 80L^2 - 4L - 2)$. Hence, at $L = 128$ there are only approximately 2×10^{10} possible locations for an error to occur, and therefore any error rates less than $1/n_p$ implies that on average no errors occur within the circuit. This shows that although for small values of L the maximum values of p and σ decrease exponentially with increasing L , they will eventually run into this polynomial lower bound. Hence in order to determine the stability of the QPF subroutine we need a more detailed look at error effects near this lower bound.

IV. STABILITY UNDER A FIXED NUMBER OF ERRORS

The next set of simulations aim to investigate the behaviour of the QPF subroutine at low discrete error rates, close to the $1/n_p$ bound. The simulations were performed in a half-stochastic, half-deterministic manner. We still allow the type and location of discrete errors to occur at random, however we now specify exactly how many errors can occur within a given run of the subroutine. Each $f(k)$ used for this section was again as shown in table (II). We now only examine the probability of obtaining the specific useful value $j = \lfloor 2^{2L}/6 \rfloor$. The specific value of j examined only effects the value (1 or 0) being measured after each modular multiplication gate and the arbitrary phase angle θ in equations (9,10). The scrambling of the $\{\alpha_j\}$ and $\{\beta_j\}$ sets caused by gate errors cannot be avoided by changing the specific value of j examined or the period. Figure (5) show the results of these simulations. Once

QPF subroutine under fixed number of errors for various values of L.

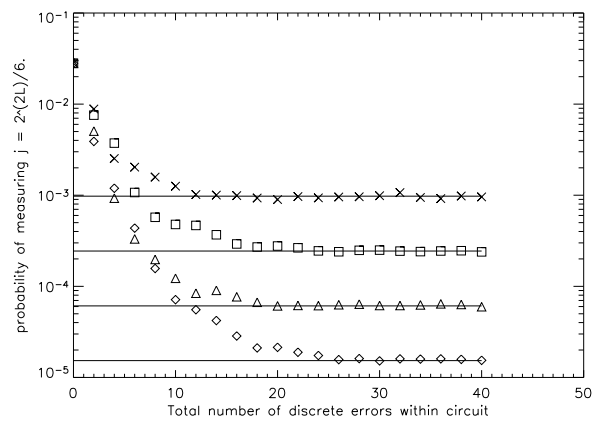


FIG. 5: Plot showing how the probability of measuring $j = \lfloor 2^{2L}/6 \rfloor$ decreases from its maximum, error free value to complete failure as a function of the specific number of errors each circuit is exposed to. The curves represent $L = 5$ to $L = 9$. Note the horizontal lines show the point of complete failure for each successive value of L .

again each data point on this plot is the average value of a

number of statistical runs for the same reasons as stated previously. Figure (5) shows us quite conclusive behaviour for the QPF subroutine at small error rates. Each curve begins at the error free probability of approximately 0.028 and decreases quite sharply as we increase the number of errors. If we define a circuit to be working if it produces non-random output (i.e if the probability of measuring a particular value of j lies above the line of complete failure) and the tolerance p_{tol} as the maximum number of errors such that the circuit is working, for the low values of L investigated it is clear that the p_{tol} is approximately 10. p_{tol} for $L = 5$ is slightly lower (about 8 errors) while p_{tol} for the $L = 8$ circuit is slightly higher (about 20 errors). From this data it appears that as we increase L to $L + 1$, the new circuit is able to tolerate perhaps two or three extra errors on average than the previous circuit. Therefore, although the QPF subroutine cannot tolerate a large number of errors without failing as shown in the initial simulations of figures (3,4) it typically does not fail when exposed to a single random error. If we assume that when going from L to $L + 1$, p_{tol} can increase by 2 on average, this translates into a p that is approximately two orders of magnitude above the $1/n_p$ lower bound for the $L = 128$ circuit. Hence, assuming this scaling for large values of L , it is possible to have a working circuit for error rates significantly higher than the $1/n_p$ lower bound. However, such an error rate would lead to a value of s that scales as $O(1/2^{2L})$ resulting in an exponential run time for Shor's algorithm, $O(1/s)$. To maintain polynomial runtime for the algorithm, figure (5) implies that p must be within an order of magnitude of $1/n_p$.

V. BEHAVIOUR FOR CIRCUITS EMPLOYING ARBITRARY INTERACTIONS

The previous simulations have examined how the linear nearest neighbour QPF subroutine behaves when exposed to gate errors. A clear extension is to look at the behaviour of an equivalent circuit not restricted to nearest neighbour interactions. As with the LNN design we assume that if the pairs are isolated, gate operations can be done simultaneously. Basically this should give an indication as to whether the stability for a LNN design is better or worse when exposed to errors than circuits not requiring the large number of swap operations to maintain nearest neighbour interactions. The error behaviour for this circuit is investigated in precisely the same way as for the LNN circuit. Figure (6) shows an equivalent plot to figure (5) for the original Beauregard circuit (modified slightly to $2L + 4$ qubits to avoid doubly controlled gates). As expected the error behaviour is largely indistinguishable from figure (5). However, there is a slight difference in p_{tol} when compared to the LNN results. This can be attributed to the slight difference in both circuits and to the statistical nature in how the above results are simulated. For example, if we consider a single error within the entire circuit, we can define $s_A^{(1)}$ as the average probability of success for the LNN circuit while $s_B^{(1)}$ be the average probability of success for the

QPF subroutine under fixed number of errors for various values of L .

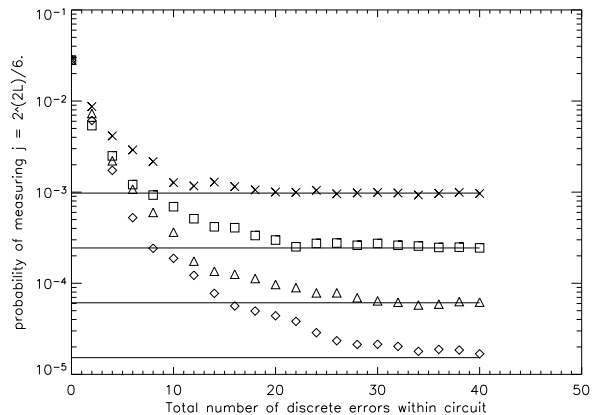


FIG. 6: Plot showing how the probability of measuring $j = \lfloor 2^{2L}/6 \rfloor$ decreases from its maximum, error free value to complete failure as a function of the specific number of errors each circuit is exposed to. Each curve represents values of L from $L = 5$, to $L = 9$. Note the horizontal lines show the point of complete failure for each successive value of L . This plot is for the original Beauregard circuit [12]

non-LNN circuit for a single random error. In this case,

$$\begin{aligned} s_A^{(1)} &= \frac{1}{3n_A} \sum_{i,j} P_{ij} + \frac{1}{3n_A} \sum_{l,j} P'_{lj} \\ s_B^{(1)} &= \frac{1}{3n_B} \sum_{i,j} P_{ij}. \end{aligned} \quad (13)$$

Where $j \in \{X, Z, XZ\}$ and n_A and n_B is defined as the number of possible locations an error can occur in the LNN and non-LNN circuits respectively. Finally let P_{ij} represent the probability of success for a given circuit when an error j occurs at location i . A simple method to analyse the difference in our results is to assume that every value of P_{ij} for the non-LNN circuit has an equivalent P_{ij} in the LNN circuit. Referring to the LNN circuit design [15] [figures (8,9,10)], there are some locations that are not present in the non-LNN design. Hence the values P'_{lj} represent terms exclusive to the LNN circuit. Substituting $s_B^{(1)}$ into $s_A^{(1)}$ gives,

$$s_A^{(1)} = \frac{n_B}{n_A} s_B^{(1)} + \frac{1}{3n_A} \sum_{l,j} P'_{lj}. \quad (14)$$

We make one final assumption regarding this second term in equation (14). The extra error locations in the LNN circuit occurs for sections such as the mesh gate, figure (9). During these sections ancilla qubits are generally reset to $|0\rangle$. X and XZ errors will then act to damage out calculation while Z errors will have no effect. Therefore, assume that for 2 of the 3 possible values of j in equation (14), $P'_{l(X,XZ)} = P_{\min} = (0.5)^{2L}$ while for Z errors $P'_{lZ} = s_B^{(0)} = P_{\max} = 0.028$. This gives,

$$s_A^{(1)} = \frac{n_B}{n_A} s_B^{(1)} + \frac{1}{3} \left(1 - \frac{n_B}{n_A}\right) (2P_{\min} + P_{\max}). \quad (15)$$

This analysis can be extended to multiple errors. For q errors it can be shown that,

$$s_A^{(q)} = \frac{1}{\Theta_{n_A}^q} \sum_{k=1}^q \frac{\Theta_{n_B}^{q-k} \Theta_{n_A-n_B}^k}{3^k} [s_B^{(q-k)} + (3^k - 1)P_{\min}] + \frac{\Theta_{n_B}^q}{\Theta_{n_A}^q} s_B^{(q)}, \quad \Theta_a^b = \binom{a}{b}. \quad (16)$$

The above derivation again assumes the following,

1. Any X or XZ error in the additional section of the LNN circuit causes the circuit to output P_{\min} .
2. If v errors (all Z) occur in the extra section of the LNN circuit, then the output of the circuit will be equivalent to the non-LNN circuit when exposed to $q - v$ errors.

In limiting cases equation (16) behaves as expected. If $n_B = n_A$ then $s_B^{(q)} = s_A^{(q)}$, as q increases, $s_A^{(q)} \rightarrow s_B^{(q)} \rightarrow P_{\min}$ and if $q = 1$, equation (16) reduces to equation (15). This analysis gives an indication as to why our simulation results for the LNN and non-LNN circuits differ. Exactly how much these circuit results vary for low values of q depends on the ratio of n_B/n_A . Simply substituting in $n_{(A,B)} = (2L + 4) \times (\text{depth})_{(A,B)}$ is not quite enough to account for the separation of these two results. However, this does show that the difference between the two circuits is not dominated by the large number of swaps within the circuit that are combined with neighbouring gates (such as controlled phase gates). Rather the difference is caused by these additional sections of the LNN circuit and the effect of these sections on the average value of success.

VI. IMPLICATIONS FOR QEC

Our simulations have shown that the QPF subroutine is highly sensitive to both continuous and discrete gate errors. For discrete errors, if we assume that the error behaviour for large values of L follows the same trend shown in these simulations, the maximum value for p such that polynomial run-time is preserved appears to be at most one order of magnitude above the $1/n_p$ lower bound. Using this information, we can now take a brief look at the demands on QEC. If we utilise the theoretical scaling behaviour [2] of k -level concatenated error correction codes such as the 7 qubit Steane code [4], and assume that our quantum computer operates at a physical discrete error rate of approximately $p = 10^{-5}$, we can construct a table showing, for large values of L , how many layers of error correction are needed and the minimum number of physical qubits required. Note that the actual physical error thresholds and scaling behaviour for the 7 qubit code is based on calculations used for a correction circuit utilising arbitrary interactions. A LNN circuit has been simulated for a 5 qubit correction code demonstrating scaling behaviour for certain values of the physical error rate [19]. Simulations need to be conducted for the 7 qubit Steane code for an appropriate LNN circuit in order to estimate if

L	p_R	k	p_{logical}	Q
64	9.3×10^{-9}	3	1×10^{-12}	45276
128	5.8×10^{-10}	3	1×10^{-12}	89180
256	3.6×10^{-11}	3	1×10^{-12}	176988
512	2.3×10^{-12}	4	1×10^{-20}	2468228
1024	1.4×10^{-13}	4	1×10^{-20}	4926852
2048	8.9×10^{-15}	4	1×10^{-20}	9844100

TABLE III: Table showing QEC requirements for the QPF subroutine. L denotes the binary length of the number to be factored. p_R is the required error rate on each logical qubit, taken to be approximately 10 times the single error rate, $p_R = 10/64L^4$. k is the number of levels of concatenated error correction. p_{logical} is the actual logical error rate for k levels of concatenated QEC using the scaling relationship $p_{\text{logical}} = (cp)^{2^k}/c$ with $p = 10^{-5}$ and $c = 10^4$. Q is the minimum number of qubits required within the circuit to factorise an L bit number using k levels of concatenated error correction $Q = (2L + 4)7^k$.

the values calculated in table (III) remain accurate. Table (III) shows, using our current simulation data that in order to factorise numbers of binary length $L = 128$ upwards, we require approximately 3^{rd} level concatenated error correction.

Since the error rate required for each logical qubit is highly dependent on the $1/n_p$ lower bound, by minimising the area of the circuit used for the QPF it may be possible to raise this lower bound and reduce the concatenation level to 1^{st} or 2^{nd} order. Table III also assumes a threshold of $1/c = 10^{-4}$. Careful circuit design could result in this value increasing and again lowering the concatenation level required.

VII. CONCLUSION

Further work is required in order to relate the results of these simulations to physical parameters of specific quantum computer architectures, e.g, relating parameters such as dephasing and decoherence times back to values of p and/or σ . Detailed simulations of 7 qubit QEC codes appropriate for a LNN design will need to be performed in order to make more accurate estimates of the demands of QEC for the results presented here.

In conclusion we have shown through detailed simulations that the QPF subroutine for Shor's algorithm is highly sensitive to both discrete and continuous errors. We have demonstrated that on average the algorithm can only tolerate discrete error rates approximately one order of magnitude above the single error lower bound for the particular circuit used. This suggests that substantial quantum error correction is necessary for factoring problems large enough to be interesting. Error rates of physical gate operations and operational times of complete circuits (with error correction) will need to be investigated further in order to be confident that a physical implementation of the QPF subroutine and hence Shor's algorithm is possible and performs in a manner

that is practical.

VIII. ACKNOWLEDGEMENTS

The authors would like to thank the staff at the Melbourne centre for high powered computing, without their facilities

simulations would have not been possible.

This work was supported by the Australian Research Council, and the Army Research Office under contract DAAD19-01-1-0653

-
- [1] P.W. Shor. Polynomial-Time Algorithms for Prime Factorization and Discrete Logarithms on a Quantum Computer. *Society for Industrial and Applied Mathematics*, 26:1484, 1997.
- [2] Nielsen and Chuang. *Quantum Computation and Quantum Information*. Cambridge, Second edition, 2000.
- [3] ARPA. Quantum information science and technology roadmap project. <http://qist.lanl.gov>, 2004.
- [4] A. M. Steane. Error correcting codes in quantum theory. *Phys. Rev. Lett.*, 77:793, 1996.
- [5] H. Imai J. Niwa, K. Matsumoto. Simulations of Quantum Error-correction Schemes. *quant-ph/0402196*, 2002.
- [6] A.Fowler and L.C.L Hollenberg. Scalability of Shor's algorithm with a limited set of rotation gates. *accepted by Physical Review A*, *quant-ph/0306018*.
- [7] X. Hu F. Nori L.F. Wei, X. Li. Phase-Matching approach to eliminate the dynamical phase error in Shor's algorithm. *quant-ph/0305039*, 2003.
- [8] E. Knill, R. Laflamme, H.N. Barnum, D.A. Dalvit, J.J. Dziazmaga, J.E. Gubernatis, L. Guruits, G. Ortiz, and W.H. Zurek. From factoring to Phase Estimation. *Los Alamos Science*, 27:38, 2002.
- [9] C. Lavor, L.R.U. Manssur, and R.Portugal. Shor's Algorithm for Factoring Large Integers. *quant-ph/0303175*, 2003.
- [10] V. Vedral, A. Barenco, and A. Ekert. Quantum Networks for Elementary Arithmetic Operations. *Phys. Rev. A*, 54:147, 1996.
- [11] P. Gossett. Quantum carry save arithmetic. *quant-ph/9808061*, 1998.
- [12] Stephane Beauregard. Circuit for Shor's algorithm using $2n+3$ qubits. *Quantum Information and Computation*, 3:175, 2003.
- [13] D.Braun. Quantum chaos and quantum algorithms *quant-ph/0110037*, 2001.
- [14] C.Zalka. Fast versions of Shor's Quantum Factoring algorithm. *quant-ph/9806084*, 1998.
- [15] A.Fowler, S.J Devitt, and L.C.L Hollenberg. Implementation of Shor's algorithm on a linear nearest neighbour qubit array. *Quantum Information and Computation*, 4:237, 2004.
- [16] Y. Makhlin. Nonlocal properties of two-qubit gates and mixed states and optimization of quantum computers. *Quantum Information Processing*, 1:243, 2002.
- [17] J.I. Cirac B. Kraus. Optimal creation of entanglement using two-qubit gate. *Phys. Rev. A*, 63:062309, 2001.
- [18] S. Sastry K.B. Whaley J. Zhang, J. Vala. Geometric theory of non-local two qubit operators. *Phys. Rev. A*, 67:042313, 2003.
- [19] A. Fowler, L.C.L. Hollenberg, and C.D Hill. Quantum error correction on linear nearest neighbour qubit arrays. *Phys. Rev. A*, 69:042314, 2004.

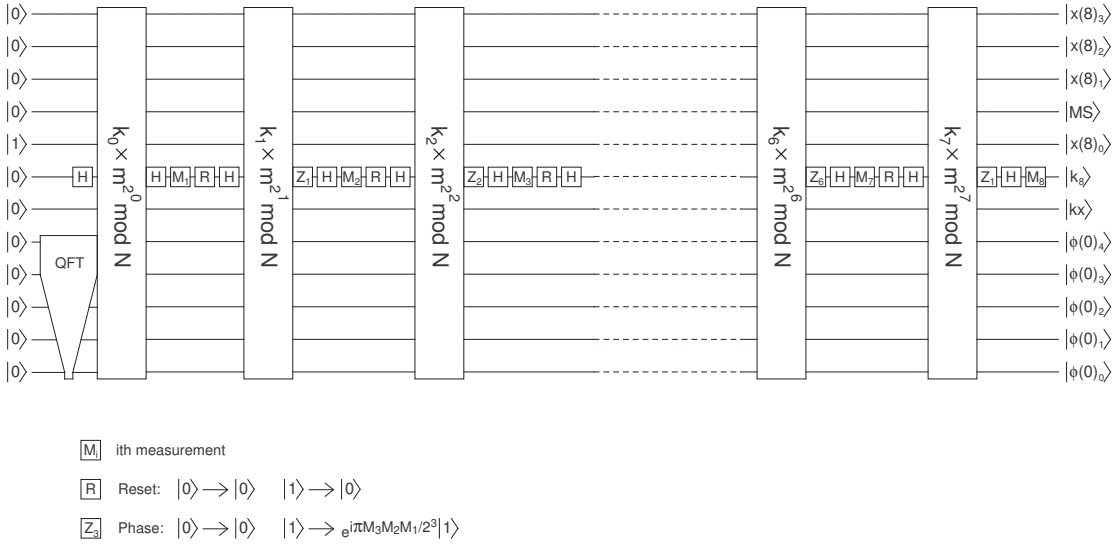


FIG. 7: Full circuit required for the QPF subroutine for 12 qubits ($L = 4$). Note that the output of the subroutine is determined through a series of measurements on a single master control qubit.

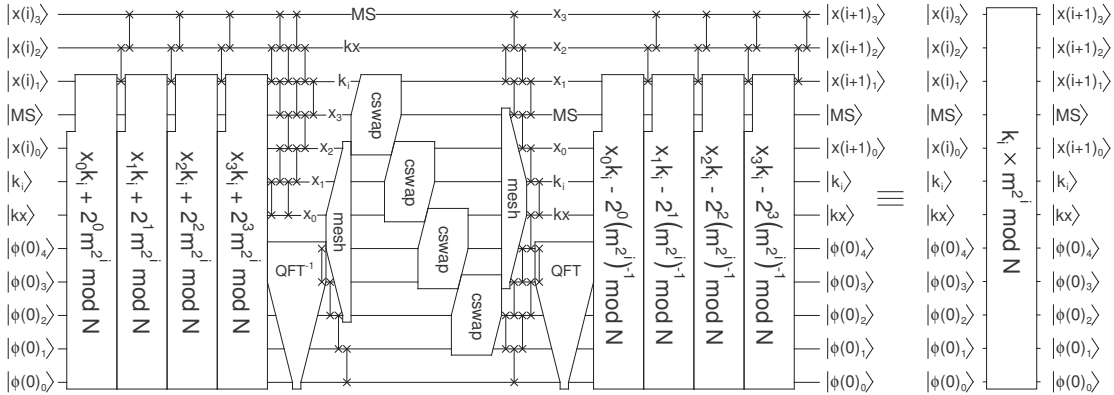


FIG. 8: Circuit required for each multiplication gate in figure (7). The middle section represents a controlled swap gate.

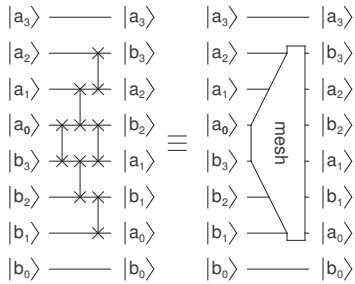


FIG. 9: Mesh circuit required for a LNN version of a controlled swap circuit. This section represents the only significant structural difference between the LNN and non-LNN circuits.

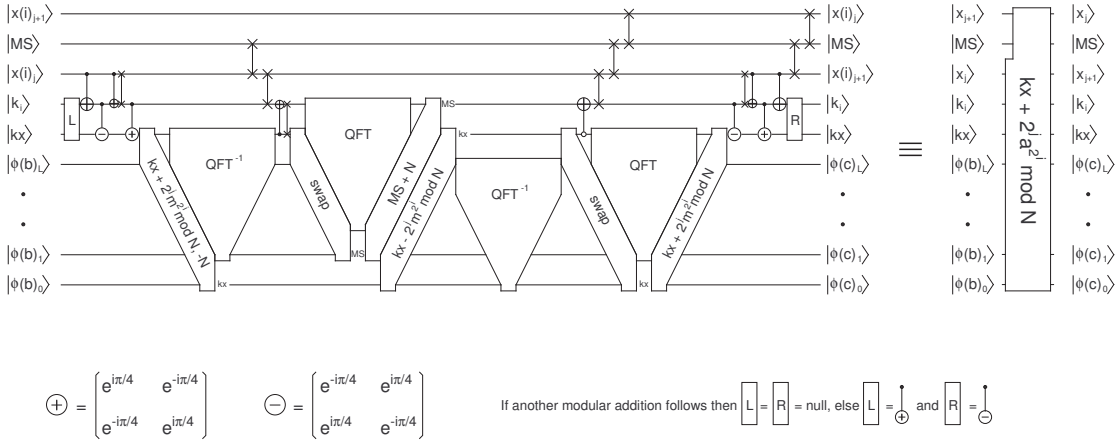


FIG. 10: Modular addition circuit required to build the multiplier gate shown in figure (8). This gate is composed of simple quantum Fourier transform gates and Fourier adders, details of these components are found in [15]